energies

MDPI

Article

Aluminium Nitride Doping for Solar Mirrors Self-Cleaning Coatings

Anna Castaldo *, Emilia Gambale and Giuseppe Vitiello

ENEA-TERIN-STSN-SCIS Portici, 80055 Naples, Italy; emilia.gambale@enea.it (E.G.); giuseppe.vitiello@enea.it (G.V.)
* Correspondence: anna.castaldo@enea.it

Abstract: Soiling severely reduces solar mirror performance, requiring dispendious water consumption for cleaning operations and causing an increase in the levelized cost of energy (LCOE). An emerging technology for facing this problem consists of developing transparent self-cleaning coatings, able to be washed with a small amount of water by virtue of the modulation of surficial wetting properties. Nevertheless, the beneficial effects of coatings decrease in the first year, and coated mirrors show even higher soiling than non-coated ones. Moreover, it is important that coating production processes are economically convenient, consistent with the intended reduction of overall costs. The aim of this work is the research and development of a cheap and scalable solution, compatible with mirror fabrication steps and, in such a sense, economically advantageous. It involves the substitution of the alumina last layer of solar mirrors with more hydrophobic, potentially auxetic aluminum compounds, such as nitrides. In particular, 2D inorganic aluminum nitride thin films doped with metals (such as aluminum and silver) and non-metals have been fabricated by means of reactive sputtering deposition and characterized for the purpose of studying their self-cleaning behavior, finding a trade-off between wetting properties, optical clarity, and stability.

Keywords: solar mirrors; aluminum nitride; sputtering deposition; self-cleaning coatings; auxetic properties

Citation: Castaldo, A.; Gambale, E.; Vitiello, G. Aluminium Nitride Doping for Solar Mirrors Self-Cleaning Coatings. *Energies* **2021**, *14*, 6668. https://doi.org/10.3390/en14206668

Academic Editor: Francesco Nocera

Received: 8 September 2021
Accepted: 12 October 2021
Published: 14 October 2021

1. Introduction

Concentrating solar power could become the cheapest form of energy production in many regions of the word, with the only problem of maintaining the solar field performance [1]. In particular, the areas of the global sunbelt, where concentrated solar power plants are typically located, suffer from high soiling due to dust accumulation, and this reduces the amount of solar energy received (and hence electricity produced), increasing LCOE [2]. The energy yield loss per day can exceed 20% if mirrored surfaces are not cleaned [3]. Fortunately, it is possible to restore their performance via washing procedures, which have to be implemented every few days, consuming water that, in some regions, is scarce and expensive. Different strategies have been proposed to solve this problem: Dry and wet cleaning, an automated or manual brush, plasma etching, anti-soiling screen layer deposition on the glass face of back surface mirrors, and so on [4].

Among the solutions, the most promising is that of coating solar mirror surfaces with self-cleaning layers, which can be hydrophobic, hydrophilic, or photocatalytic thin films, whose washing requires the smallest amount of water, reducing maintenance costs [5]. Such a strategy, however, has to preserve the optical performance of mirrors and this implies the further requirement of UV-Vis-NIR high transmittance of the coatings. So far, the only marketable solution has been commercialized by Alcan and utilizes super hydrophobic nano-textured fluoro-silane-based coatings. Flabeg [6] and Guardian both confirm that they are working on anti-soiling titania-silica hydrophilic coatings but have not announced details yet. The Dutch company Rads Global Business has developed an

anti-soiling coating for solar PV modules, which is claimed to reduce cleaning costa by around 60% [7].

Nevertheless, the beneficial effects of anti-soiling decrease over the years and coated mirrors show even higher soiling than non-coated ones [8]. There is not a unique solution valid for all types of mirrors and all climates. In this frame, it appears clear that research and development of new coatings is a topic of particular interest. In our opinion, a profitable approach is to start from materials that are already present in the last layer exposed to the air, such as aluminum oxides and substituting them with aluminum nitrides and metamaterials based on them, tailored for washing with less water.

The choice of aluminum nitride, AlN, a hard covalent semiconductor with a bandgap of 6.2 eV, whose common crystalline hexagonal phase is a wurtzite-type structure [9], results from the consideration of preserving the overall mirror fabrication process architecture. This requires changing only a few steps relative to the alumina last layer (Al_2O_3, an aluminum oxide neither hydrophilic nor hydrophobic utilized as a transparent barrier layer to preserve the stability and reflectivity of metallized mirrors) with a wetting tailorable aluminum compound, more hydrophobic than alumina (Al_2O_3). With the electropositive cation, Al^{3+} nitrogen forms covalent bonds, Al-N, with higher cohesive forces than the ionic bond of oxides. For this reason, aluminum nitride is a hard solid material in bulk form, while in thin films, there are many metastable Al_xN_y phases, whose chemistry can enable the persistence of different topological arrangements. In particular, 2D reentrant honeycomb AlN politypoyds, with a mixed tetragonal and hexagonal structure, that exhibit auxetism and photocatalytic properties have recently been discovered [10].

Auxetic materials (from the Greek word 'αὐξητικός', whose meaning is 'tending to increase') show a negative Poisson's ratio (the ratio between the transverse and longitudinal strain produced by the application of a load orthogonal to the section), related to their unusual deformation in a perpendicular direction by means of the application of mechanical stress/strain, as reported in Figure 1 [11].

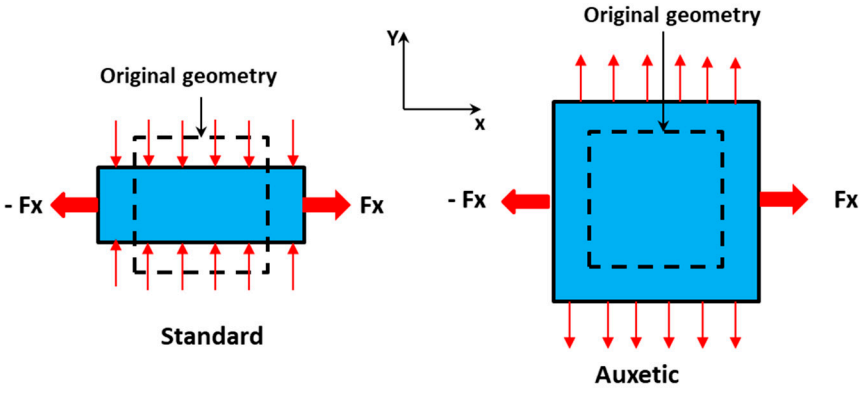

Figure 1. Standard and auxetic structures showing strain relationships and geometries when stretched.

As a classical example of auxetic materials, Gore-tex fibers, if strained, resemble an opened umbrella. Even though the existence of auxetic materials has been known for more than 150 years, only a few natural examples have been found in certain biological tissues (cat skin, cow teat, butterfly wings). Despite this, partial auxetics are quite common, as 69% of cubic elemental metals present an auxetic behavior in at least one direction. In any case, auxetic behavior is not related or specific to any particular material, being purely a consequence of how the material itself is structured microscopically [12]. There are different auxetic topologies, such as 2D reentrant honeycombs, rotating polygonals, chiral, or 3D derived from buckling. In particular, a microstructure constituted by connected equilateral triangles or squares can be auxetic when, if stressed, geometrical constituents remain rigid but rotate with respect to each other. When auxetic materials expand their surface

area, it is likely as a result of expected changes to the wetting properties of their surface. This occurs, for example, in expanded polytetrafluoroethylene (ePTFE), the microporous superhydrophobic waterproof and breathable layer in GoreTex.

Concerning the inorganic AlN auxetic structures discovered by Kilic and colleagues, it is possible, in our opinion, to fabricate them as thin films by means of reactive sputtering deposition. Experimental activity has been devoted to this goal.

It is important to underline that inorganic aluminum nitride could be more convenient than the other hydrophobic proposals for covering solar mirrors. In fact, for hydrophobic transparent coatings, the few present solutions contemplate the utilization of fluorinating production steps, which are onerous since fluorination costs and the associated *processing* are expensive [13].

Concerning AlN thin films, they can be produced via various methods, including molecular beam epitaxy (MBE), electron cyclotron resonance dual-ion beam sputtering, pulsed laser ablation, and metal organic chemical vapor deposition (MOCVD), which all require high processing temperatures and are also expensive [14]. Direct current (DC) reactive sputtering deposition, utilized in this work as the production method, has the advantage of being a low-temperature, low-cost, easily scalable technique, useful for depositing thin films of different compositions on glass and polymeric substrates, under the conditions of kinetic control without any transformation in equilibrium phases, as described in a previous work [15].

Here, exploiting previous expertise on 2D metamaterials for spectrally selective coatings able to mirror solar heat toward the Universe [16], a range of 2D inorganic and hybrid thin-film metamaterials have been developed. So, different coatings with potential auxetic and photocatalytic properties based on aluminum nitride doped with metals (silver, aluminum, tungsten) and non-metals (oxygen, nitrogen) have been fabricated by means of sputtering These are characterized by means of different techniques and are proposed as anti-soiling and self-cleaning coatings for solar mirrors, considering that the change in surface area with a strain induced by metamaterial fabrication processes (2D growth on proper templates) combines with hydrophilic and hydrophobic properties to manipulate the overall wetting properties of the surfaces. In particular, this study takes into account the effect of combining modified wettability with the requirements of preserving a solar mirror coating's [17] optical reflectance and appropriate durability over time [18].

2. Materials and Methods

Coatings produced in this work are mono- or multi-layered, deposited by means of the reactive sputtering technique, using a proprietary multi-cathode apparatus equipped with magnetron and dual-magnetron cathodes operating in DC or pulsed DC and in the medium frequency mode, respectively.

For greater clarity in identifying manufactured samples, Table 1 shows the sample identification names, distinctive experimental fabrication conditions (such as total pressure (P_0 in mbar) and reactive gas flow (in sccm)), and the thickness of coatings.

Ag ultrathin layers were grown in DC sputtering mode at an Ar pressure of 1.0×10^{-3} mbar and with 1.65 W/cm^2 power density applied to the Al cathode. AlN layers were grown by means of reactive sputtering at an Ar + N_2 pressure ranging from 1.0×10^{-2} to 4.4×10^{-4} mbar with a power density of 7.75 W/cm^2 applied to the Al cathode.

Al_2O_3 film was deposited by means of reactive sputtering at an Ar + O_2 pressure of 1.0×10^{-3} mbar with a power density of 7.75 W/cm^2 supplied to the Al cathode.

The thickness of single layers was measured by means of a Surface Profiler TENCOR P-10.

UV-VIS-NIR analysis was performed using a double-beam Perkin-Elmer mod. A Lambda 900 instrument, equipped with an integrating sphere, was used to measure global spectral reflectance and transmittance. Measurements were collected in the 200–2500 nm spectral range under ambient conditions. A halon white (PTFE) reflectance standard was used as the baseline.

Table 1. Sample nomenclature and experimental fabrication details.

Sample Identification	Composition	P0 [mbar]	Gas Flow (sccm)	Thickness [nm]
AlN_{tp}	Glass/AlN in saturation regimen	1.3×10^{-3}	200 Ar + 60 N_2	102
AlN_{pre}	Glass/AlN in transition regimen at 3000 W	1.3×10^{-3}	200 Ar + 25 N_2	82
AlN_{pre2}	Glass/AlN in transition regimen at 1500 W	1.0×10^{-3}	200 Ar + 25 N_2	80
Al_2O_3	Glass/Al_2O_3 in saturation regimen	1.3×10^{-3}	200 Ar + 50 O_2	107
AlN_{post}	Glass/AlNpre annealed at 580 °C	-	-	80
AlN_{tp2}	Glass/AlN in saturation regimen annealed at 580 °C	-	-	100
AlNx_1	Glass/AlN in transition regimen obtained with 1 sccm O_2	9.3×10^{-4}	50 Ar + 28 N_2 + 1 O_2	106
AlNx_2	Glass/AlN in transition regimen obtained with 2 sccm O_2	5.1×10^{-4}	50 Ar + 28 N_2 + 2 O_2	120
AlNx_3	Glass/AlN in transition regimen obtained with 3 sccm O_2	5.7×10^{-4}	50 Ar + 28 N_2 + 3 O_2	124
AlNx_4	Glass/AlN in transition regimen obtained with 4 sccm O_2	5.2×10^{-4}	50 Ar + 28 N_2 + 4 O_2	100
AlNx_4 bis	Glass/AlN in transition regimen obtained with different reactive gas mixture/Argon ratio	4.4×10^{-4}	400 Ar + 7 O_2 + 50 N_2	97
AlN_Ag1	Glass/AlN/Ag/AlN	1.0×10^{-3}	400 Ar + 40 N_2	37/8/47
AlN_Ag2	Glass/AlN/Ag16 nm/AlN	1.0×10^{-3}	400 Ar + 40 N_2	37/16/47

Vibrational analysis of materials was performed by means of micro-RAMAN and FTIR techniques. Fourier Transform Infrared (FTIR) spectra were recorded with a Bruker Fourier transform spectrometer model Equinox 55, equipped with a Deuterated triglycine sulphate detector operating in the 400–4000 cm^{-1} range and an MCT detector operating in the 560–8000 cm^{-1}. The resolution was 4 cm^{-1}. Raman spectra were collected with a Renishaw visible Raman spectrometer system, equipped with a confocal microscope. Laser excitation at 514 nm (green) was supplied by a YAG double-diode pumped laser (20 mW).

The Static Water Contact Angle (WCA) was measured with the direct optical method of drop-shape analysis, by means of the contact angle meter KRUSS DSA-100.

The same Renishaw mod. inVia Raman spectrometer equipped with a 514 nm Argon ion laser and an 1800 L/mm grating was used to collect photoluminescence (PL) spectra in the 540–950 nm range.

Annealing tests were performed by exposing samples in a vacuum environment to thermal cycles at the temperatures of 470 °C (AlN_{post}) and 560 °C for 8 h (AlN_{pre2}, AlN_{post2}).

Photocatalytic behavior was evaluated by means of a thin-film exposition test adapted from the normed method ISO10678, consisting of exposing samples immersed in a solution of Methylene Blue to UV lamp (253 nm) irradiation for 90 min and measuring the absorption of the chromophore at 653 nm before and after the test. The organic dye in the presence of UV radiation was degraded by photolysis promoted by the tested samples, which act as photo-catalysts.

3. Results and Discussion

In order to change solar mirrors' wettability for the purpose of reducing water consumption and hence costs in cleaning operations and maintenance (O&M), experimentation on thin-film metamaterial coatings based on aluminum compounds different from oxides was conducted. In particular, we studied the promotion of auxetic properties in sputtered politypoids of aluminum nitride, by means of 2D growth and doping with metals (such as

aluminum, silver) and/or non-metals (such as nitrogen and oxygen) for the purpose of demonstrating modulation of wetting properties of the alumina last layer of solar mirrors.

The first important consideration concerns the nitridation reaction for obtaining AlN by means of reactive sputtering deposition starting from the metallic aluminium target. In the reactive sputtering, nitridation occurs between the metallic target and reactive nitrogen added to the argon processing gas. There are different possible operating regimens: Metallic, transition, and saturation of the sputtering aluminum target, dependent on the reactive gas concentration. They differ for the change from the metallic (where metallic aluminum is ejected from the target and nitridation occurs on the substrate) to compound mode (defined saturation regimen, or poisoned mode, where the reaction occurs on the target and nitrides are then ejected from the poisoned target), passing through a transition regimen (where unstable, partially nitridated target is operative) of the material sputtered from the target. The cathode voltage and deposition rate vary from the metallic to saturation regimen, where the reach their minimum level, remaining constant even with an increasing N_2 concentration. Despite different operational varieties, by means of reactive sputtering deposition in different regimens, a hexagonal, equilibrium-phase (wurtzite) crystalline structure is easily obtained in thick samples. For thin and ultrathin film composition, crystallite orientation and domain dimensions can be influenced by the sputtering regimen.

This work is devoted to study this aspect for the purpose of fabricating auxetic metamaterials. A careful study on the growth conditions of "constrained equilibrium", where the formation of the equilibrium phase is kinetically inhibited (strategies toward the direct synthesis of metastable compounds), has been conducted to address the promotion of auxetic surfaces with different wettability, where geometrical crystalline polygonal micro-domains have a topological spatial disposition and an overall shape useful for accommodating deformation and/or reticular enlarging.

Thin films of AlN in this work have been produced by means of reactive sputtering in two different macro-conditions: High and medium content of reactive gas (saturation and transition regimens), characterized by means of Raman spectroscopy, FTIR, photoluminescence, and RX analysis.

The first structural comparison comes from micro-Raman analysis of aluminum nitride thin films obtained with a large amount of available nitrogen in the saturation regimen (AlN_{tp}) with a minor nitrogen concentration in the transition regimen (AlN_{pre}), reported in Figure 2. A difference in Raman activity of samples obtained in two regimens can be observed.

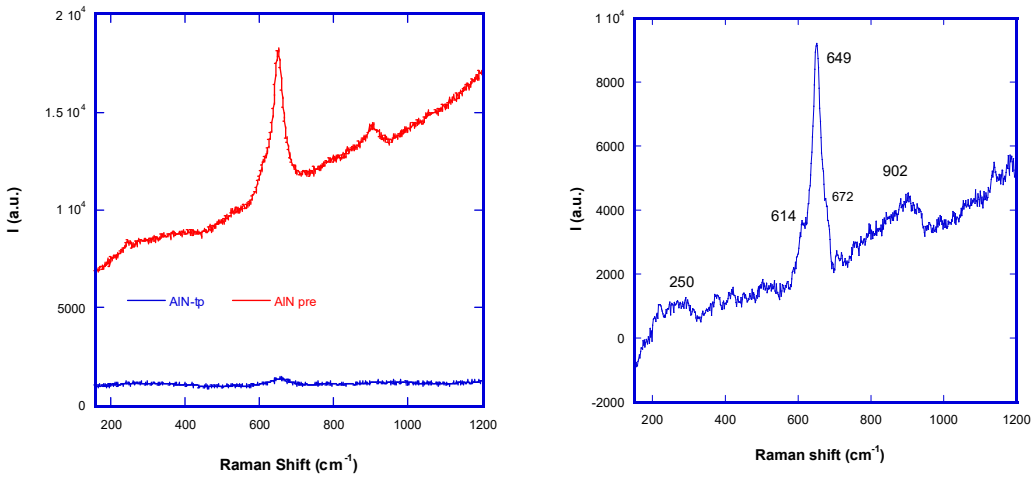

Figure 2. Micro-Raman analysis of thin AlN films deposited in two different regimens. (**a**) Comparison of Raman activity. (**b**) AlN_{pre} thin-film vibrational analysis.

Group theory predicts AlN in eight vibrational modes: 2E2, 2A1, 2E1, and 2B1, all of which, except the silent B1, are Raman active: 252 cm^{-1}, 614 cm^{-1}, 658 cm^{-1}, 672 cm^{-1}, 894 cm^{-1} e 912 cm^{-1} for the hexagonal phase and 658 cm^{-1} (TO) and 912 cm^{-1} (LO) for the cubic zinc-blend phase.

The Raman spectrum of the transition regimen AlN_{pre} (Figure 2b) has three peaks: 250 cm^{-1} (broad), 649 cm^{-1} (intense and coalescent with 614 cm^{-1} and 672 cm^{-1}), and 902 cm^{-1} (broad), and this means that there are both phases (hexagonal and cubic, as foreseen for auxetic Th-AlN). The Raman frequency position for stress-free bulk AlN is 657.4 cm^{-1} and such an E^2_2 mode can be used to detect the stresses in the plane (σ_{xx}) and on the c plane (σ_{zz}) of AlN, by means of the relationship:

$$\Delta\omega_\lambda = 2\alpha_\lambda\varepsilon_{xx} + b_\lambda\varepsilon_{zz} = 2\check{\alpha}_\lambda\sigma_{xx} + \check{b_\lambda}\sigma_{zz}$$

where α_λ and β_λ are deformation potential constants and ε is the strain [19]. The Raman stress factor is an energy difference (or a frequency shift, with respect to the relaxed frequency position). In AlN_{pre}, there is a blue shift to 649 cm^{-1} that can be related to tensile stress (stress factor k = $-6.361.4$ cm^{-1}/GPa for the E2 mode). AlN_{tp} obtained in the saturation regimen has lower Raman activity with a unique peak at 655 cm-1 (stress factor k = -2.4 cm $-$ 1/GPa for the E2 mode) and broad bands in the region of nitrogen molecule bond stretching (around 2300 cm^{-1} RS).

In particular, the peak of the multiple nitrogen bonds stretching at around 2320 cm^{-1} (the nitrogen molecule in the gas phase has such stretching at 2354 cm^{-1} Raman Shift) in the Raman spectrum (Figure 3) can be attributed to AlN rings, where there are N = *n* bonds predicted in simulations on the th-AlN phases.

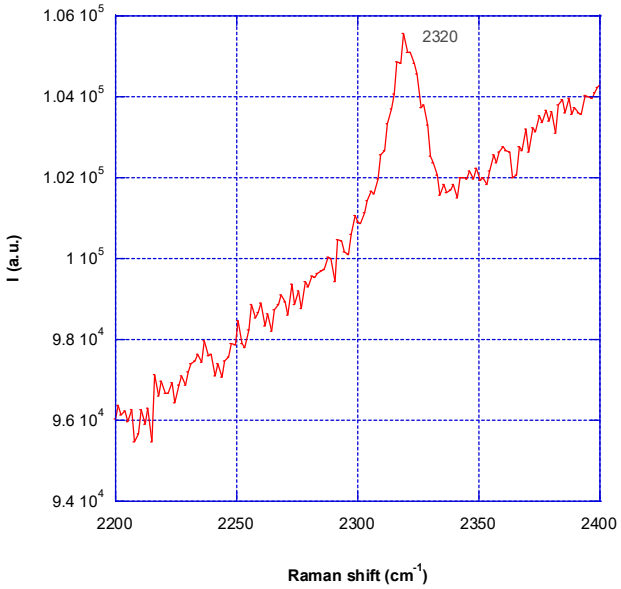

Figure 3. Micro-Raman spectrum of AlN_{pre}, peak of the nitrogen multiple bonds in the region (2200–2400 cm^{-1}).

It is possible that the produced AlN_{tp} is a mixed th AlN cubic phase. In general, the Raman activity of AlN_{pre} is higher than AlN_{tp} for the SERS effect due to the presence of metallic aluminium clusters.

In other words, concerning the transition region, under-stoichiometric AlN has been produced, with amorphous aluminium islands. Meanwhile, in the saturation regimen, the material sputtered from a completely poisoned target is super-stoichiometric AlN_y, hosting a certain amount of partially reduced nitrogen in the lattice. In both cases, micro Raman data confirm the presence of auxetic phases.

FTIR analysis (Figure 4) performed in the reflectance mode in the range 570 ÷ 700 cm^{-1} shows the two signals for Al-N stretching at 622 cm^{-1} (TO) and 851 cm^{-1} (LO), a small peak at 1004 cm^{-1}, attributable to the Al_2N cluster (or *n* bonding 2 Al^{3+} ions), a broad band at 1246 cm^{-1}, for Al = *n* and Al ≡ *n* (multiple bonds presence indicates that there is an auxetic phase), an intense 1435 cm^{-1} band relative to N-H bending, and 2881 cm^{-1} and 3615 cm^{-1} bands of combined stretching for -OH e $-NH_x$.

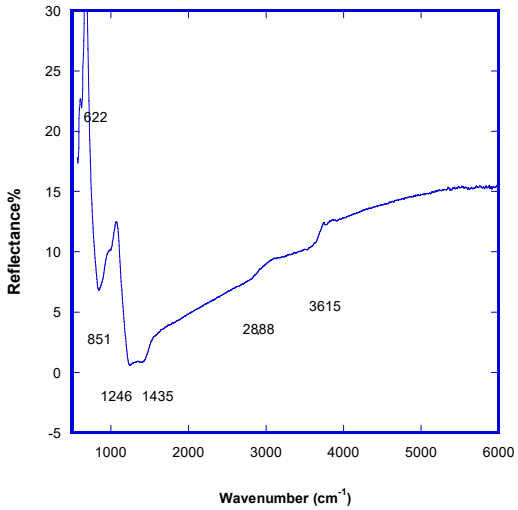

Figure 4. FTIR AlN_{pre} analysis.

Theoretical infrared active Al-N bond stretching frequencies are 655 cm^{-1} (TO) and 860 cm^{-1} (LO). The two signals are both visible when the material is a bulk crystal, with prominence in the LO mode. Moreover, TO is visible only when crystallites are randomly oriented with respect to the substrate (no c-axis). In such an experimental case, the lattice is distorted along the c axis and the bond in AlN has a mixed ionic and covalent character, because TO and LO experimental modes are more distant than those reported in the literature. In conclusion, FTIR analysis confirms the presence of Al_xN clusters in transition-regimen AlN_{pre} samples, which means not all aluminum was nitridated and the resulting metamaterial was a nitride doped with aluminum, AlN_Al.

From both analyses, interesting experimental evidence of multiple bonds in the obtained AlN thin films (either between aluminium and nitrogen, or between two nitrogen atoms) was obtained, and this is in accord with the spatial arrangement of multiple bonds with neighbors (due to the valence electron pair repulsion rule) constituted by ordered hexagonal and tetragonal rings with unprecedented properties (anisotropy, a negative Poisson's ratio, ultrahigh ideal strength, photo-catalytic properties, tunable wettability, etc.).

To test the structural stability of the obtained metamaterials, high-temperature annealing of the thin films as sputtered was performed in two steps: The first annealing at 470 °C for six hours, followed by sample characterization and then second annealing at the higher temperature of 580 °C for 8 h.

Figure 5 reports the comparison between the photoluminescence of samples obtained in two sputtering regimens before (AlN_{pre} and AlN_{tp}) and after (AlN_{post} and AlN_{tp2}) the annealing step at 580 °C. First of all, the thin films produced were all photo-luminescent and presented different photo-emissive defects. A relatively wide emission band was observed, which ranges from 540 nm (2.29 eV) to 900 nm (1.38 eV), centered at 738 nm (1.68 eV). It is noteworthy that as the 514 nm laser was below the bandgap for AlN, the observed PL originated from defects as a result of the vacancy of aluminum and/or O impurities that substitute nitrogen (O_N). In particular, comparing both AlN_{tp} and AlN_{tp2} curves (samples produced in saturation before and after annealing) and AlN_{pre} and AlN_{post} curves (samples produced in the transition regimen before and after annealing), it is possible to observe

that the O_N (1.93 eV) defect increases after annealing, and nitrogen-metal related defects N_{Al} (1.4–1.85 eV) decrease because there is an oxygen "contamination".

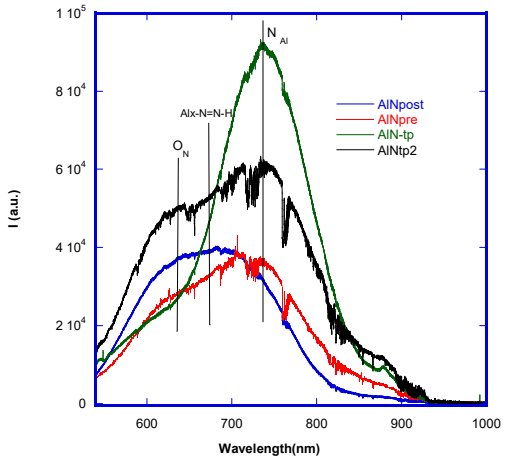

Figure 5. AlN thin-film photoluminescence spectra before (AlN_{pre} and AlN_{tp}) and after (AlN_{post} and AlN_{tp2}) annealing at 580 °C.

After the annealing, both kinds of samples (transition and saturation) modified their photo-emissive trend in terms of intensity and peak positions. It is likely that the nanometric aluminum clusters that are under-nitridated and dispersed in the crystalline AlN lattice undergo oxidation during annealing, increasing the concentration of oxygen defects. Oxygen has a high affinity toward aluminum, due to an atomic radius smaller than nitrogen, so the AlN lattice has a high capability of accommodating oxygen without phase segregation. To preserve the system's electro-neutrality, aluminum vacancies are created. When the oxygen concentration increases, there is first a reduction in the reticular parameter and then an expansion of the cell volume. At a critical point, the two defects (V_{Al} and O_N) are combined to become one single octahedric defect, nulling the two vacancies.

Moreover, Al_x-N = N-H photo-emissive complexes are evident and imputable to metallic clusters, which arise during nitridation processes when there is a surplus of reactive nitrogen and thermal energy coming from the heating of the substrate. These findings confirm that there are micro-structural differences between samples that can be influenced by thermal treatments, and that, generally, samples obtained in the transition regimen are more defected and hence more photoluminescent.

The XRD analysis reported in Figure 6 shows a crystalline nature with a mixed structure: Tilted (101) and columnar (002), as previously described [19]. After the first annealing at 470 °C, the peak intensities increase, in particular for the (002), and the overall crystallinity grows. Such modification is due to excess nitrogen removal. The following 580 °C annealing does not introduce any further modification and/or recrystallization.

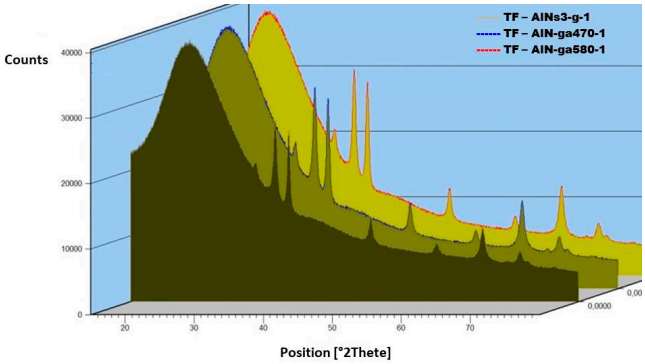

Figure 6. AlN_{pre} RX analysis before and after two annealing steps.

To Summarize, the analyses conducted have demonstrated that sputtered AlN thin films have different compositions, micro-structures, and a certain indefinite number of oxygen and aluminum clusters, which can be considered doping elements. When the target operates in the metallic regimen, there is a high deposition rate, high cathode voltage, and the presence of aluminum clusters in a hexagonal lattice of AlN. Upon increasing the nitrogen concentration, the target operates in a transition regimen where the cathode voltage and deposition rate slightly decrease and the film's composition tends towards a stoichiometric Al/N ratio, the microstructure varies, and a mixed-phase hexagonal-cubic structure appears. Finally, in the saturation regimen, the cathode voltage and deposition rate are at their minimum and do not change with nitrogen concentration, the AlN hexagonal lattice hosts the nitrogen in excess, there are no aluminum clusters, and there is evidence of a mixed th-phase.

Concerning the wetting behavior, as previously hypothesized, alumina is more hydrophilic than nitrides (Table 2). A thin alumina film produced by means of reactive sputtering in saturation regimen of reactive oxygen from the same aluminum target has a WCA of 61° (alumina of commercial solar mirrors has a WCA of around 50°). The two different nitride thin films (AlN_{pre} and Al_{tp}) have different wetting properties and, in particular, AlN_{pre} is more hydrophobic than Al_{tp}. This difference can be slightly reduced after the annealing step that produces Al-O bonds, as previously demonstrated.

Table 2. Water contact angle (WCA) of thin aluminum compound films.

Sample	WCA
AlN_{tp}	95 ± 4
AlN_{pre}	100.8 ± 1.5
AlN_{post}	97.9 ± 0.5
Al_2O_3	61 ± 4

In both cases, nitride thin films confirm the hydrophobic character that is highly desired in this frame.

After the morphological and chemical-physical characterization, UV-Vis-NIR analysis was conducted to verify the optical clarity necessary to grant mirrors good optical performance. In particular, it is important that when passing from alumina to nitrides there is no significant loss in optical transmittance to ensure that mirrors' reflectivity can be preserved. Figure 7 reports the transmittance, reflectance, and absorbance for alumina and the three nitride thin films of similar thickness. As can be observed, alumina is more transparent than nitrides in the visible range because the band gap is too large to absorb visible light due to the deep valence band (O 2*p* orbitals) positions. Nitrogen has a lower electronegativity than oxygen, so the substitution of oxygen with nitrogen results in a substantial increase in the bonding covalence and visible light absorption. Moreover, the optical properties of nitrides can vary largely by controlling their stoichiometry, which determines changes in the density of free electrons. The enhanced transmittance of the AlN_{pre2} film is due to the total pressure increase combined with the power decrease, with both conditions determining a decrease in particle energies during the deposition, and hence a less defective structure (compared to the photo-emissive behavior previously described). Upon decreasing the defect concentration, it is possible to increase transmittance in the region of 500–700 nm, finding a trade-off between wettability and optical properties.

Therefore, AlN_{pre2} obtained in the transition regimen can be considered a good starting point for future experimentations on a larger scale.

Considering that Al-O bonds confer optical clarity but a worsening of wetting properties, it may be convenient to introduce oxygen in a more controlled way in the sputtering process. A definitive amount of this gas has been added to nitrogen (from 1 sccm to 4 sccm) during the reactive sputtering process, obtaining a family of doped AlN metamaterials, named AlN_x, that are more transparent than AlN, as expected (cf. Figure 8), and remain hydrophobic (Table 3), with WCA close to 100°.

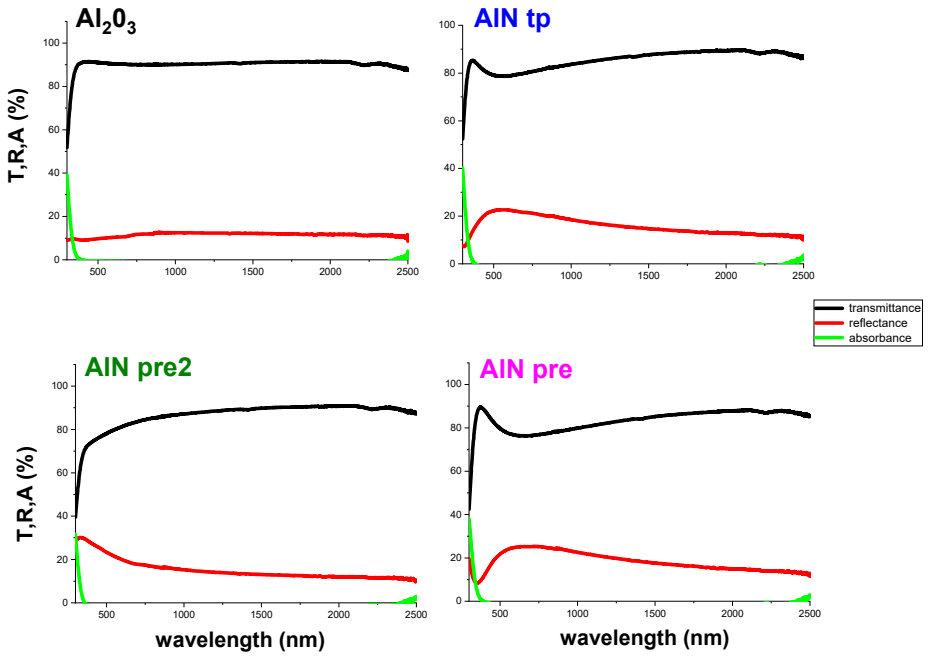

Figure 7. UV-Vis-NIR analysis of aluminum compounds thin films: Alumina, AlN_{tp}, AlN_{pre2}, AlN_{pre}.

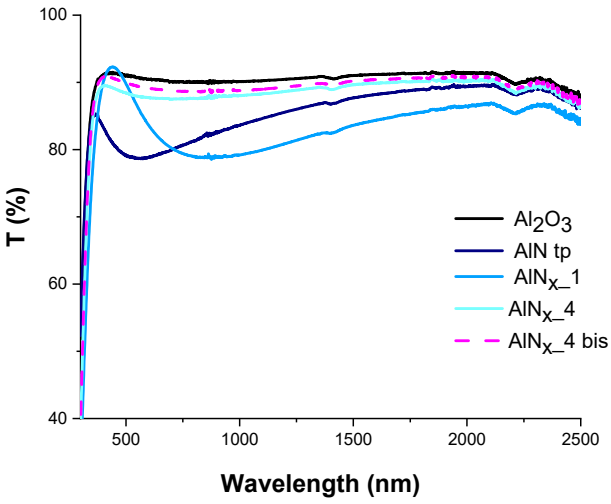

Figure 8. UV-VIS-NIR transmittance of aluminum nitride thin films compared to alumina.

Table 3. WCA of oxygen-doped aluminum nitride thin films.

Sample	WCA
AlNx_1	98 ± 3°
AlNx_2	96.3 ± 0.5°
AlNx_3	96 ± 2°
AlNx_4	98.6 ± 1.5°
AlNx_4 bis	96.0 ± 0.8°

The second approach to doping AlN to ensure auxetic behavior was performed by adding (in a definitive amount) a metallic guest in the nitride lattice. Previously, we have shown an excess of aluminum (although not in a definitive amount) is present in the transition-regimen-obtained AlN samples (e.g., AlN_{pre}), giving rise to oxidation when exposed to high temperatures. As a metallic guest, a less-oxidable homologue of aluminum is the noble metal silver. From an experimental point of view, for the purpose of preserving

a mixed tetragonal–hexagonal AlN wurtzitic lattice (which is the only recognized auxetic phase) while also introducing silver as a dopant, the chosen method is the fabrication of an ultrathin silver layer between two AlN layers, following a method already adopted in our labs for producing transparent, low-emissive coatings [20]. In particular, ultra-thin silver films grow on the AlN seed layer template, and it is then possible to freeze the structure by means of growing another thin AlN third layer. The resulting metamaterial is cermet-like AlN-Ag.

Three different layer structures have been fabricated and characterized. Such structures have hydrophobic behavior (WCA: 98°). The only drawback of this method is the lower optical clarity in the range of 900–2500 nm (Figure 9) due to silver reflectance and interferential structural effects (dielectric–metal–dielectric).

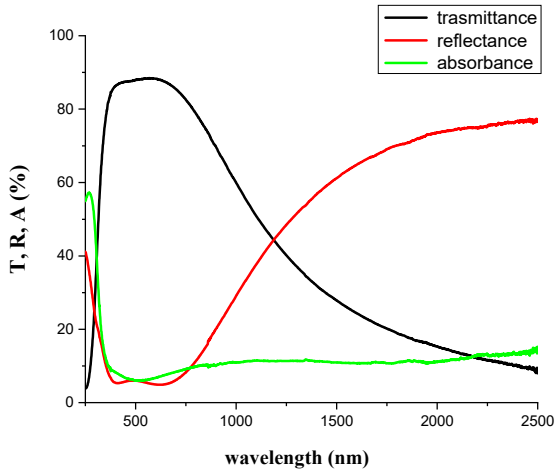

Figure 9. Transmittance, reflectance, and absorbance of AlN_Ag2 sample.

Upon reducing the thickness of the silver layer (AlN_Ag1 has a half thickness with respect to the silver layer of sample 2), it is possible to enlarge the optical clarity region, but samples with silver nano-islands result in being highly photoluminescent (cf. Figure 10).

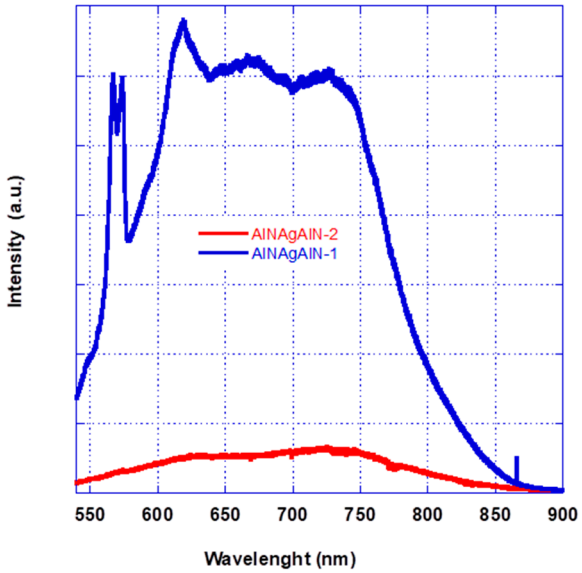

Figure 10. Thin-film photoluminescence comparison of AlN_Ag1 and AlN_Ag2 samples.

Indeed, it is possible to enlarge the optical clarity in the solar range window by acting on interferential effects that relate to the relative thickness of the three layers, by

means of a semi-empirical method already described in our work on solar thermodynamic coatings [21]. Here, an optimization of the optical performance is outside the scope, but experiments are already ongoing in such a direction.

Concerning self-cleaning behavior, the produced metamaterials have been tested to verify their photocatalytic properties by means of a test adapted from ISO10678, consisting of the immersion of thin films in a proper solution of methylene blue (BM) in the presence of UV irradiation (253 nm for 90 min) followed by the measurement of chromophore visible absorption at 653 nm, comparing data of the pristine (not degraded) dye with those of solutions exposed to the photocatalyst. Figure 11 reports the comparison between supernatant solutions where different potentially photocatalytic samples have previously been immersed. All tested materials are able to degrade methylene blue (BM) and hence organic pollutants, confirming their self-cleaning nature.

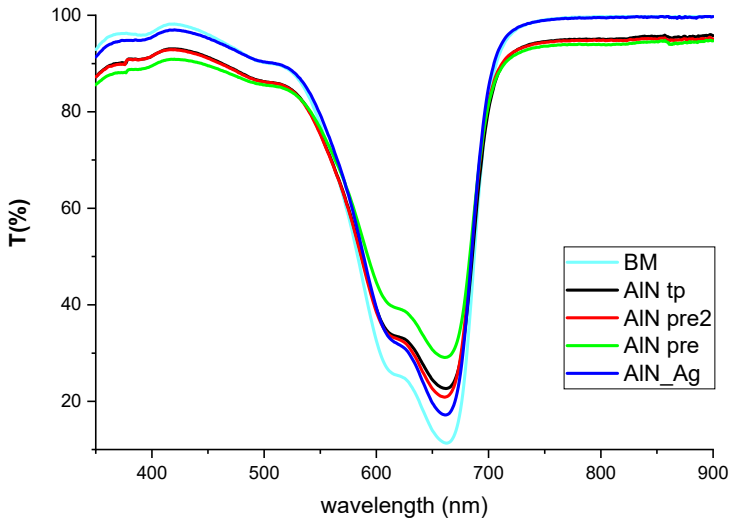

Figure 11. UV-Vis-NIR transmittance spectra of the BM dye supernatant solution after immersion tests of different thin films.

The photocatalytic behavior is further evidence of the auxetic nature of the fabricated thin-AlN-film-based metamaterials.

In conclusion, the fabrication method of doped AlN developed in this work utilizing previous expertise of our labs makes it possible to obtain metamaterials with tailorable wettability.

From the overall set of analyses, it is possible to conclude that a trade-off between hydrophobic, photocatalytic, and optical clarity abilities of doped AlN metamaterials is possible, and this represents a promising approach to change the wettability of the last alumina layer of solar mirrors.

4. Conclusions

This work illustrates the potential of using AlN-based polytypoid metamaterials to change the wettability of solar mirrors, for the purpose of reducing water consumption in O&M and hence LCOE produced in concentrated solar power plants. In particular, it has been shown to be possible to change the wettability (from 61° to 100° WCA), promoting auxetic and photocatalytic properties in sputtered metamaterials, by means of mixed-phase polycrystalline nitrides 2D growth and doping with metals (such as aluminum and/or silver) and non-metals (such as nitrogen and/or oxygen), preserving optical clarity in the visible solar range. It is possible to find a trade-off between wetting performance and optical properties, granting appropriate durability over time.

In conclusion, via proper fabrication skills, self-cleaning metamaterials have been tailored, produced, characterized, and selected to function in a solar range. A similar

original approach that combines hydrophobic and photocatalytic effects is promising for the goal of a significant reduction of water consumption in solar mirrors and their cleaning and maintenance. The proposed solution is cheap, scalable, and has a potentially easy integration in already-existing production lines of commercial solar mirrors.

Author Contributions: Conceptualization, A.C. and E.G.; methodology, A.C. and E.G.; data curation, E.G. and G.V.; writing—original draft preparation, A.C.; writing—review and editing, A.C. All authors have read and agreed to the published version of the manuscript.

Funding: The results presented in this paper have been obtained in the framework of the project "Concentrating Solar Power", under the "Electric System Research" Programme 2019-2021, with the financial support of Italian MITE, Italian Ministry of Ecological Transition.

Conflicts of Interest: The authors declare no conflict of interest.

References

1. IEA. World Energy Outlook 2020, IEA, Paris. 2020. Available online: https://www.iea.org/reports/world-energy-outlook-2020 (accessed on 20 September 2021).
2. Pennetta, S.; Yu, S.; Borghesani, P.; Cholette, M.; Barry, J.; Guan, Z. An investigation on factors influencing dust accumulation on CSP mirrors. *AIP Conf. Proc.* **2016**, *1734*, 070024–070031.
3. Wette, J.; Fernández-García, A.; Sutter, F.; Buendía-Martínez, F.; Argüelles-Arízcun, D.; Azpitarte, I.; Pérez, G. Water saving in CSP plants by a novel hydrophilic anti-soiling coating for solar reflectors. *Coatings* **2019**, *9*, 739. [CrossRef]
4. Wolfertstetter, F.; Wilbert, S.; Dersch, J.; Dieckmann, S.; Pitz-Paal, R.; Ghennioui, A. Integration of soiling-rate measurements and cleaning strategies in yield analysis of parabolic trough plants. *J. Sol. Energy Eng.* **2018**, *140*, 041008–041011. [CrossRef]
5. Jang, G.G.; Smith, D.B.; Polizos, G.; Collins, L.; Keum, J.K.; Lee, D.F. Transparent superhydrophilic and superhydrophobic nanoparticle textured coatings: Comparative study of anti-soiling performance. *Nanoscale Adv.* **2019**, *1*, 1249–1260. [CrossRef]
6. Available online: https://www.flabeg.com (accessed on 20 September 2021).
7. Available online: https://www.radsglobal.nl (accessed on 20 September 2021).
8. Aranzabe, E.; Azpitarte, I.; Fernández-García, A.; Argüelles-Arízcun, D.; Pérez, G.; Ubach, J.; Sutter, F. Hydrophilic anti-soiling coating for improved efficiency of solar reflectors. *AIP Conf. Proc.* **2018**, *2033*, 220001. [CrossRef]
9. Prohaska, G.; Miller, G. Aluminum Nitride: A review of the knowledge base for physical property development. *MRS Proc.* **1989**, *167*, 215. [CrossRef]
10. Kilic, M.E.; Lee, K.-R. Auxetic, flexible, and strain-tunable two-dimensional th-AlN for photocatalytic visible light water splitting with anisotropic high carrier mobility. *J. Mater. Chem. C* **2021**, *9*, 4971–4977. [CrossRef]
11. Ren, X.; Das, R.; Tran, P.; Ngo, T.D.; Xie, Y.M. Auxetic metamaterials and structures: A review. *Smart Mater. Struct.* **2018**, *27*, 023001. [CrossRef]
12. Dagdelen, J.; Montoya, J.; de Jong, M.; Persson, K. Computational prediction of new auxetic materials. *Nat. Commun.* **2018**, *18*, 323–331. [CrossRef] [PubMed]
13. Varshney, P.; Mohapatra, S.S.; Kumar, A. Superhydrophobic coatings for Aluminium surfaces synthesized by chemical etching process. *Int. J. Smart Nano Mater.* **2016**, *7*, 248–264. [CrossRef]
14. Haussonne, F.J. Review of the synthesis methods for AIN. *Mater. Manuf. Proc.* **1995**, *10*, 717–755. [CrossRef]
15. Addonizio, M.L.; Ferrara, M.; Castaldo, A.; Antonaia, A. Air-stable low-emissive AlN-Ag based coatings for energy-efficient retrofitting of existing windows. *Energy Build.* **2021**, *250*, 111259–111269. [CrossRef]
16. Castaldo, A.; Vitiello, G.; Gambale, E.; Lanchi, M.; Ferrara, M.; Zinzi, M. Mirroring solar radiation emitting heat toward the universe: Design, production, and preliminary testing of a metamaterial based daytime passive radiative cooler. *Energies* **2020**, *13*, 4192. [CrossRef]
17. Hunter, S.R.; Smith, D.B.; Polizos, G.; Shaeffer, D.; Lee, D.F.; Datskos, P.G. Low cost anti-soiling coatings for CSP collector mirrors and heliostats. In *High and Low Concentrator Systems for Solar Energy Applications IX*; International Society for Optics and Photonics: Bellingham, WA, USA, 2014; Volume 9175, p. 91750.
18. Profokieva, T.; Seon, M.; Vanbuskirk, J.; Holtz, M. Vibrational properties of AlN grown on <111>-oriented silicon. *Phys. Rev. B* **2001**, *63*, 125313–125320.
19. Antonaia, A.; Esposito, S.; Addonizio, M.L.; Guglielmo, A. Solar Selective Absorber Based on Double Nitride Composite Material and Process for Its Preparation. Patent IPN WO/2012/172505, 1 December 2012.
20. Ferrara, M.; Castaldo, A.; Esposito, S.; D'Angelo, A.; Antonaia, A. AlN–Ag based low-emission sputtered coatings for high visible transmittance window. *Surf. Coat. Technol.* **2016**, *295*, 2–7. [CrossRef]
21. Esposito, S.; D'Angelo, A.; Antonaia, A.; Castaldo, A.; Ferrara, M.; Addonizio, M.L.; Guglielmo, A. Optimization procedure and fabrication of highly efficient and thermally stable solar coating for receiver operating at high temperature. *Sol. Energy Mater. Sol. Cells* **2016**, *157*, 429–437. [CrossRef]